Dependence of the Adsorption of Chiral Compounds on their Enantiomeric Composition.

ARTICLE *in* SURFACE SCIENCE · FEBRUARY 2014

Impact Factor: 1.93 · DOI: 10.1016/j.susc.2014.02.003

3 AUTHORS, INCLUDING:

Stavros Karakalos
Harvard University
33 PUBLICATIONS **67** CITATIONS
SEE PROFILE

Francisco Zaera
University of California, Riverside
372 PUBLICATIONS **11,953** CITATIONS
SEE PROFILE

Surface Science 629 (2014) 3–10

Contents lists available at ScienceDirect

Surface Science

journal homepage: www.elsevier.com/locate/susc

Dependence of the adsorption of chiral compounds on their enantiomeric composition

Alexander D. Gordon [1], Stavros Karakalos, Francisco Zaera *

Department of Chemistry, University of California, Riverside, CA 92521, USA

ARTICLE INFO

Available online 9 February 2014

Keywords:
Enantioselectivity
Kinetics
Infrared absorption spectroscopy
Temperature programmed desorption
Naphthylethylamine
Propylene oxide
Platinum

ABSTRACT

The adsorption of two different chiral molecules on platinum surfaces has been explored as a function of enantiomeric composition. In the first case, the saturation monolayers obtained by the adsorption of 1-(naphthyl) ethylamine (NEA) from CCl_4 solutions were characterized in situ by reflection–absorption infrared spectroscopy (RAIRS). It was found that racemic mixtures yield different IR spectra than those obtained from enantiopure monolayers, a behavior that was interpreted as the result of the formation of racemate pairs via hydrogen bonding at the amine moiety also responsible for bonding to the surface. NEA adsorption under these conditions is reversible and can be modified by subsequent exposures to solutions of different chiral compositions, but that appears to take place only via changes in the relative fractions of enantiopure versus racemic domains on the surface; no other enantiomeric ratios are apparent in the IR data. The second study focused on the uptake of propylene oxide (PO) on Pt(111) under ultrahigh vacuum (UHV) conditions. In that case, racemic monolayers show densities up to ~20% lower than those obtained with one single enantiomer. This can be explained by kinetic arguments, since data from isothermal molecular-beam experiments indicated that the PO sticking coefficient depends on the chirality of the incoming PO molecules relative to that of the neighboring adsorbed PO species. Monte Carlo simulations could reproduce the experimental data by assuming adsorbate-assisted adsorption and enantiospecific adsorption geometries for molecules impinging on sites adjacent to previously adsorbed surface species.

1. Introduction

Chemical chirality is ubiquitous in nature, and central to the biochemistry of life. In our desire to control certain aspects of that biochemistry, as is the case in the development of pharmaceuticals or agroproducts, for instance, we need to be able to exert control on the chirality and enantioselectivity of the chemicals involved. As a consequence, there is a great interest in finding ways to synthetize chiral compounds and in separating their individual enantiomers. Much chemistry has been advanced toward this goal in solution, but much less is known and understood about the chemistry of chiral compounds on surfaces [1–3].

The adsorption of chiral molecules on metal surfaces has received some attention from the surface-science community in recent years. Many chiral molecules have been shown to adopt complex ordered adsorption patterns on single-crystal surfaces depending on their total coverage and on the enantiocomposition of the adsorbed mixture. Interesting symmetry breaking has been reported in some cases, induced either by chiral seeding [4–6] or via amplification of small imbalances in enantiomeric composition [7–9]. These observations may have significant implications for the design of schemes for the enantiopurification of chiral compounds via preferential crystallization [10].

The use of small amounts of chiral molecules has also been evaluated as a way to bestow enantioselectivity to heterogeneous catalysts, typically to hydrogenation catalysts based on transition metals [11–13]. The best, and basically only, examples of such imparting of enantioselectivity on catalysts via the addition of chiral modifiers are those with tartaric acid on nickel-based catalysts [14] and with cinchona alkaloids on platinum-based catalysts [15,16], in which a C═O double bond in a prochiral molecule is hydrogenated to yield the chiral product. In the latter case, it is believed that the structure of the modifier provides a chiral pocket for complexation with the reactant, which may possibly occur via strong interactions such as hydrogen bonding [17]. That is assumed to be followed by adsorption of the reactant–modifier complex on the surface of the catalyst in a particular geometry and by the consequent biasing of the hydrogenation step toward one of the two possible enantiomeric products [18,19]. With tartaric acid as the chiral modifier, on the other hand, this one-to-one reactant–modifier complexation may not be sufficient, and enantioselectivity may require more extended supramolecular structures. In fact, supramolecular chiral templating of surfaces has also been proven possible with small chiral adsorbates by chiral titration experiments with a second probing molecule, typically

* Corresponding author.
E-mail address: zaera@ucr.edu (F. Zaera).
[1] Present address: Oak Ridge National Laboratory, Chemical Sciences Division, Oak Ridge, TN 37831-6110, USA.

0039-6028/$ – see front matter © 2014 Elsevier B.V. All rights reserved.
http://dx.doi.org/10.1016/j.susc.2014.02.003

propylene oxide [20–24]. In that case, the argument has been that surface chiral pockets may result form specific geometrical arrangements of the adsorbates on the substrate. Typically, no additional forces are at play, but in some cases strong intermolecular interactions such as hydrogen bonding may be required as well [25].

Our knowledge on the adsorption of chiral molecules by themselves is still quite limited. As indicated above, chiral resolution based on crystallization forces has been identified in ordered systems, and strong intermolecular interactions such as hydrogen bonding have also been observed in heterochiral systems on surfaces. Yet, the role of those properties on the formation of chiral monolayers of adsorbates is poorly understood. Here we report on two different systems where the adsorption of chiral molecules varies depending on their enantiocomposition. For both 1-(1-naphthyl)ethylamine (NEA) [23] and propylene oxide (PO) [26] on platinum surfaces, different adsorption modes and/or coverages have been observed with enantiopure versus racemic mixtures. The reasons behind these differences seem to be several, but do not appear to require the involvement of long-range order, and, at least in the case of PO, do not include strong intermolecular interactions either. Below, we expand on the results from these studies.

2. Experimental details

Two types of experiments are reported here, carried out with two different instruments. The study on the adsorption of 1-(1-naphthyl) ethylamine (NEA; Sigma-Aldrich, >99% purity) was performed by using a reflection–absorption infrared spectroscopy (RAIRS) cell designed for in situ studies of adsorption from solution [27] where a thin liquid film of the solution of interest is trapped between a polished polycrystalline Pt disk and a transparent trapezoidal CaF_2 prism used as the optical element to guide the IR beam in and out of the system. The Pt disk was cleaned in situ before each experiment by electrochemical oxidation–reduction cycles in 0.1 M $KClO_4$ for 1 h. The reported spectra correspond to differences between data obtained with p- and s-polarized light to discriminate between adsorbed species (which show up only in the p-polarized data) and molecules in solution (visible in both p- and s-polarized spectra), after ratioing against the equivalent p–s background data obtained with the pure solvent. All the reported spectra correspond to averages from 256 scans, taken with 4 cm^{-1} resolution. Deionized water, used as a solvent, was purified in house; all other solvents (CCl_4, toluene, ethanol, acetone) were purchased from Sigma-Aldrich and used as received.

The second set of experiments, on the adsorption of propylene oxide (S-, R-, and Rac-PO; Sigma-Aldrich, 99% purity; 98 D atom % in Rac-PO-d_6) on a Pt(111) single-crystal surface, was performed in a ultrahigh-vacuum (UHV) instrument equipped with a UTI mass spectrometer, placed at the back of the chamber and interfaced to a personal computer, which was employed for gas identification and detection and for temperature-programmed desorption (TPD) and isothermal molecular-beam kinetic measurements (for which an effusive collimated beam was also used) [28,29]. The surface of the Pt sample was cleaned before each experiment by a combination of ion sputtering and O_2 treatments. Linear heating rates of 10 K/s were used for the TPD experiments by using a homemade temperature controller, and constant fixed temperatures were set for the molecular beam uptakes. Exposures in these experiments are reported in units of Langmuirs ($1\ L = 1 \times 10^{-6}$ Torr s), with pressures measured by using a nude ion gauge (not corrected for ion gauge sensitivity factors).

Density functional theory (DFT) calculations (Fig. 1) were carried out for the assignment of the infrared absorption frequencies in the NEA IR absorption spectra by using the B3LYP method and the 6–311 + G(2d, p) basis set [30]. The Monte Carlo simulations carried out for the second system were performed using a home-written routine in Matlab, using "L" shaped molecules surrounded by a one-lattice-space frame to prevent adsorption of molecules directly touching each other, and two separate intrinsic sticking probabilities (S_o) for adsorption on empty

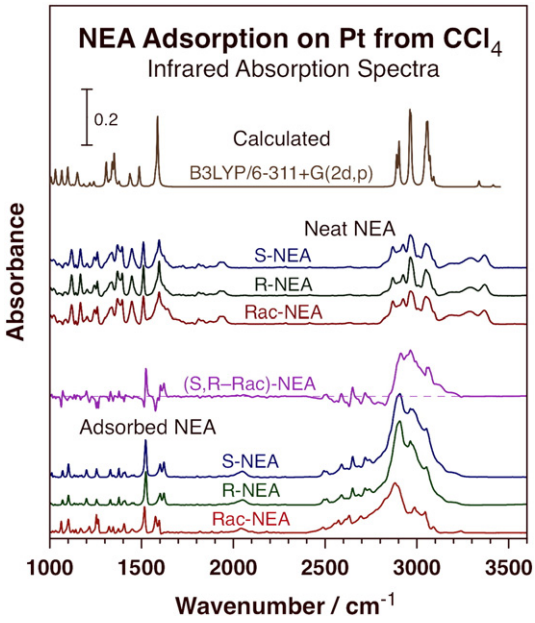

Fig. 1. Bottom four traces: In-situ reflection–absorption infrared spectra (RAIRS) for S-, R-, and racemic-1-(1-naphthyl)ethylamine (NEA) adsorbed onto a polished polycrystalline platinum surface from 500 μM CCl_4 solutions at room temperature, and the differential spectra obtained by subtracting the trace for the Rac-NEA from an average of the S- and R-NEA data. To notice here are the differences between the trace for the racemic mixture and those for the enantiopure layers (highlighted in the differential trace), in particular in the 1500–1700 cm^{-1} region. Next three traces from bottom: Equivalent transmission IR spectra for the same S-, R-, and Rac-NEA but in neat liquid form. No differences are seen in those cases. Top trace: Calculated IR spectrum for NEA, obtained by using the B3LYP method and the 6–311 + G(2d,p) basis set.

versus occupied sites [26]. Specific adsorption geometries were also defined for the incoming molecules hitting on adsorbates depending on their relative handedness (S–S or R–R versus S–R or R–S) [26].

3. NEA adsorption onto a Pt surface from solution

Our first study was carried out with 1-(1-naphthyl)ethylamine (NEA). This is a relatively simple chiral molecule that nicely represents the chiral modifying chemistry of cinchona alkaloids in catalysis. NEA possesses the main functionalities required for the formation of one-to-one reactant–modifier complexes in such systems, namely, an aromatic ring and an amine group near a chiral center [23,31–33], and has also shown to be able to add some enantioselectivity to the catalytic hydrogenation of α-ketoesters [34–36]. Several surface-science studies have focused on the adsorption of NEA on Pt and Pd surfaces [23,37–40], but, to the best of our knowledge, there have been no comparative studies on the adsorption of NEA as a function of the relative amounts of R- versus S-enantiomers on the surface. This is the behavior that we discuss below.

The bottom four traces of Fig. 1 correspond to RAIRS data from saturated layers of S-, R-, and racemic- (Rac-) NEA adsorbed on a polycrystalline Pt surface, and to the difference between the average of the S- and R-NEA spectra minus the trace for the Rac-NEA. These spectra were obtained in situ upon adsorption from 500 μM NEA solutions in a CCl_4 solvent. The data for the S- and R-NEA enantiomers are, within experimental error, identical, but those obtained with Rac-NEA show a number of distinct features not seen with the enantiopure layers (highlighted in the differential spectrum), indicating a potential difference in pairwise interactions between molecules of the same versus different chirality on the surface. Perhaps the most noticeable difference is in the pair of peaks detected around 1600 cm^{-1}: with the enantiopure layers two features are centered around 1600 and 1622 cm^{-1}, whereas the racemic mixture shows those at 1575 and 1597 cm^{-1}. Other changes in the 1000–1700 cm^{-1} (molecular deformations) frequency range

include redshifts of the 1070, 1330, 1410, and 1522 cm^{-1} features, to 1062, 1322, 1404, and 1517 cm^{-1}, respectively, a blueshift of the peak at 1200 cm^{-1} to 1215 cm^{-1}, and a change in relative intensities in the doublet at 1252/1264 cm^{-1}. In the C–H stretching (2700–3200 cm^{-1}) region, the feature at 2900 cm^{-1} with the enantiopure NEAs redshifts to 2880 cm^{-1} in the racemic sample, and that at 2965 cm^{-1} blueshifts to 2988 cm^{-1}.

In order to better understand the changes induced by the variations in the enantiocomposition of the NEA adsorbed layers, the RAIRS peaks need to be assigned to specific vibrations. Interpretation of the NEA IR spectra has already been reported in the past [23,38], but a closer look was required to analyze the new results in Fig. 1. To that end, the IR spectrum of isolated NEA molecules was simulated here using DFT calculations. The result, shown in the top trace in Fig. 1, agrees reasonably well with the experimental data obtained for neat NEA, shown for the pure S, pure R, and racemic mixture in the second, third, and fourth traces from the top in Fig. 1, respectively. It should be noted that no differences were seen among the IR spectra of the enantiopure versus racemic NEA samples in the neat liquid phase, as in the adsorbed layers. Previous work also failed to identify any differences among NEA layers adsorbed under UHV conditions [23].

Perhaps the most informative piece of evidence from the simulated IR spectra of NEA is that, although most peaks in the 1500–1700 cm^{-1} region are due to naphthalene ring deformation modes, there is a hidden feature at 1587 cm^{-1} (in the simulated spectrum), underneath the strong signal at 1576 cm^{-1}, due to the scissoring mode of the NH_2 moiety (γ_{NH_2}). It may very well be that the latter IR band splits and/or shifts in frequency upon NEA adsorption. This seems particularly viable here because a recent report from our laboratory has pointed to the fact that bonding of NEA from CCl_4 solutions to Pt surfaces takes place at the amine group [40]. Additional DFT calculations showed that this peak splitting does indeed occur with ammonia, in which case the single γ_{NH_2} feature calculated at 1606 cm^{-1} for one isolated NH_3 molecule splits into two bands at 1606 and 1634 cm^{-1}. We suggest that the amine group in NEA may hydrogen-bond with an adjacent adsorbate, and that such interaction is different with homochiral versus heterochiral NEA pairs. In fact, it does appear as if S/R NEA racemate pairs may form on the Pt surface. Similar arguments related to shifts in the γ_{NH_2} frequency upon hydrogen bonding on Pt surfaces were offered by McBreen and coworkers in their interpretation of the behavior of NEA coadsorbed with methyl pyruvate [38]. Additional support for our interpretation comes from the general observation that the most noticeable differences in the IR spectra of the adsorbed S- or R- versus Rac-NEA, beyond those associated with the NH_2 moiety, are in the 1070/1062, 1330/1322 and 1410/1404 cm^{-1} features, all associated with the non-aromatic part of the molecules (the ν_{C-CH_3}, δ_{CH} + δ_{s,CH_3}, and δ_{a,CH_3} modes, respectively). Some changes in the orientation of the aromatic ring are also evident by the changes seen in the 1522/1517 cm^{-1} peak and in the 1252/1264 cm^{-1} pair.

The possible pairwise interactions that determine the differences seen in the IR spectra for NEA between enantiopure and racemic mixtures on Pt surfaces must not be very strong, since they are reversible. This was shown by displacement experiments, in which either enantiopure or racemic NEA monolayers were exposed to solutions with a different NEA enantiocomposition (racemic or enantiopure, respectively). Typical raw IR data from these studies are shown in Fig. 2, in that case for an experiment where an initial monolayer of enantiopure S-NEA, prepared via exposure of the clean Pt surface to a 500 μM S-NEA-in-CCl_4 solution, was subsequently exposed to a series of similar fresh solution of Rac-NEA (9 in total in this example), after which pure S-NEA solutions were used again (10 cycles in Fig. 2). The changes in the enantiocomposition of the adsorbed NEA layers are evident by the changes in the appearance of the corresponding RAIRS data, in particular in the relative variations in intensity of the 1600/1622 (S-NEA) versus 1575/1597 (Rac-NEA) cm^{-1} pairs of peaks. Interestingly, the fact that only the relative intensities of those peaks but not their

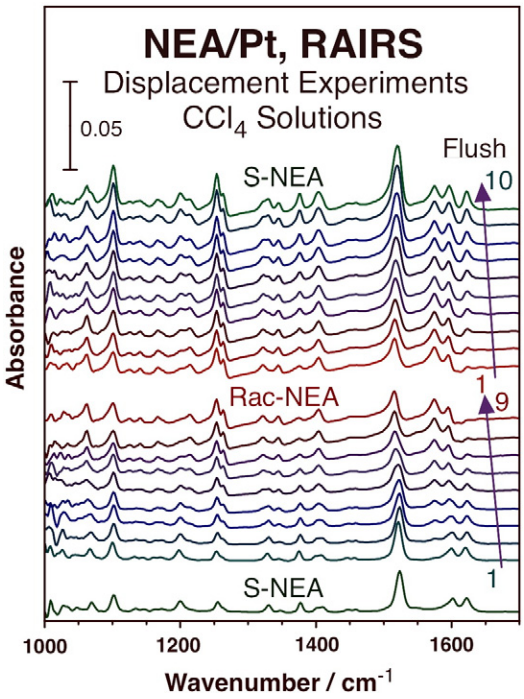

Fig. 2. RAIRS from displacement experiments with S- and Rac-NEA. The Pt surface was sequentially exposed to 500 μM CCl_4 solutions of (from bottom to top) S-NEA, Rac-NEA (9 times), and S-NEA again (10 times). A total transformation from S-NEA to Rac-NEA layers is evident in the first half of these experiments, but only a slower and incomplete conversion back to the enantiopure layer is observed in the second half. No evidence is seen of new types of mixed layers, suggesting that the intermediate spectra correspond to mixtures of separate domains of S- and Rac-NEA adsorbates on the Pt surface. The total NEA monolayer coverage is also seen to increase monotonically with each new exposure to a fresh NEA solution.

frequencies vary with increasing flushings with the appropriate NEA solutions indicates that no new interactions develop as the overall enantiocomposition of the adsorbed NEA layers evolves: either the intermolecular interactions are quite localized, involving only pairs of adsorbed molecules, and/or, the NEA enantiopure and racemic layers coexist in separate domains on the surface. It should be indicated that other, more subtle, changes are seen in these spectra as well (a slight change in shape and position of the feature at ~1520 cm^{-1} due to a ring deformation mode, for instance). Nevertheless, all of those changes can be ascribed to differences between the spectra of the enantiopure versus racemate adsorbates; again, no new IR features develop in these displacement experiments. We suggest that perhaps, because of the hydrogen bonding suggested by the data in Fig. 1, the NEA forms conglomerates of specific enantiocomposition, either with one single enantiomer or as 1:1 S-NEA:R-NEA racemates, and that the transition from one to the other occurs at the interfaces between adjacent domains.

A summary of data from displacement experiments such as those in Fig. 2 arising from quantitative analysis of the peak intensities for the estimation of surface coverages is provided in Fig. 3. The solid symbols in that figure correspond to the experiment reported in Fig. 2, whereas the open symbols originate from a similar experiment started with a racemic NEA monolayer, which was then exposed to pure S-NEA solutions first and to Rac-NEA solutions again afterward. The relative S-NEA and R-NEA coverages were estimated by deconvolution of the IR peak intensity signals for the 1575 (Rac-NEA) and 1622 (S-NEA) cm^{-1} peaks, assuming linear relationships between intensities and coverages and similar absorption coefficients for both vibrational modes (which was corroborated by using the extreme cases, the data for 100% S-NEA and Rac-NEA layers). Again, the changes in enantiocomposition are evident in both cases. Also to note is the fact that the original pure S-NEA monolayer can be converted to a fully racemic mixture, and that, in the

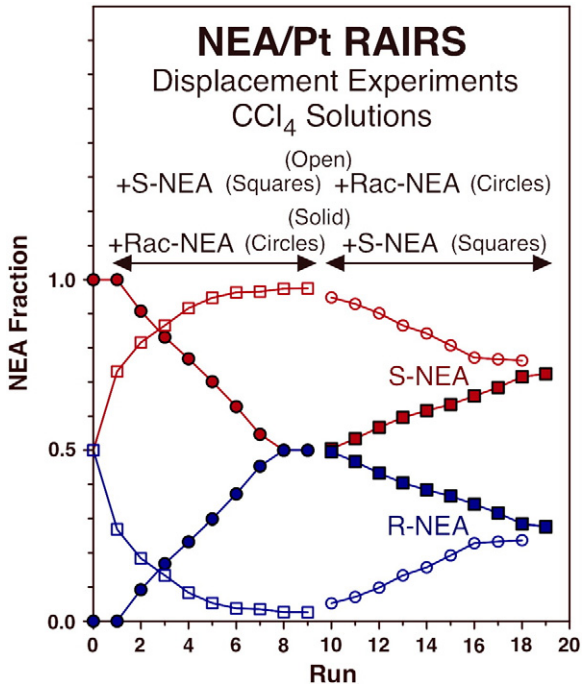

Fig. 3. Summary of relative S- (red symbols) and R- (blue symbols) NEA coverages in displacement experiments such as those exemplified in Fig. 2, for experiments starting with pure S-NEA (solid symbols) and with Rac-NEA (open symbols). The type of NEA being added in each phase of these experiments is indicated by the type of symbol used: squares when S-NEA is used, circles when Rac-NEA is employed instead. Full conversion, to Rac- and S-NEA layers, respectively, is seen after the first 10-exposure cycle, but only incomplete reversal of that conversion is attained in the second 10-exposure cycle.

same way, an initial racemic layer can transition to an enantiopure S-NEA layer, within 10 cycles of exposures to fresh Rac-NEA/CCl_4 or S-NEA/CCl_4 solutions, respectively. However, the conversion back to the original S-NEA or Rac-NEA layers is not complete, at least not after the additional 10 cycles carried out in these experiments.

The slowing down in the interconversion between enantiopure and racemic layers on the surface with increasing number of exposures to NEA fresh solutions may be explained by a concomitant increase in total coverage, as evidenced by the absolute intensities of the peaks in Fig. 2. It was estimated that the total NEA coverage on the Pt surface goes up by approximately 50% after each 10-cycle set of exposures of the surface to fresh NEA/CCl_4 solutions (for the two sets of cycles reported here at least), a behavior that was also observed in experiments where the clean Pt surface was sequentially exposed to fresh solutions of NEA of the same chirality (data not shown). It is speculated that the exchange of adsorbates with molecules from solution may require an initial adsorption of the latter on open surface sites, and that such initial step becomes more difficult as the monolayer becomes denser (as it is bound to happen after the repeated cycles of exposures to fresh solutions carried out in the experiments in Figs. 2 and 3). It should be noted that, because in these experiments the surface is exposed to a solution of the adsorbate, NEA in this case, an adsorption dynamic equilibrium should be attained in which both adsorption and desorption events take place at equal rates. This means that there is always a finite probability for exchange of adsorbates with other molecules in solution [41]; only the rate of that exchange may become slower with increasing surface coverage.

Both the desorption rate and the adsorption equilibrium of NEA on the Pt surface are affected significantly by the solvent used. Previous work in our laboratory has shown that, for a family of cinchona alkaloids and other related compounds, the adsorption equilibria depend strongly on the nature of the solvent used [42], and that a good correlation exists between this adsorption and the solubility of the adsorbate (NEA in our case here) [19,43,44], which in turn is strongly associated with the empirical polarity of the solvent [43,45]. In general, non-polar compounds are poor solvents for these chiral modifiers (including NEA), and therefore are associated with high binding constants on the surface. This was corroborated for NEA by testing the ability of the pure solvent to remove a layer of adsorbed NEA from the Pt surface. Fig. 4 shows some of the key data from those experiments. It is seen there that the initial S-NEA layer (bottom trace) remains intact on the surface after flushing with pure carbon tetrachloride or toluene (next two traces from bottom), but are easily removed by ethanol, acetone, or water (top three traces). Note that in these experiments the cell was flushed with CCl_4 after using the solvent of interest to minimize interferences from the solvents in the RAIRS traces, but that some signal from those still remained (the peaks at 1496 cm^{-1} for toluene, at 1097, 1244, 1288, 1388, and 1443 cm^{-1} for ethanol, and at 1099, 1219, and 1360 cm^{-1} for acetone). Ultimately, since CCl_4 was used as the solvent for most of the experiments reported here, the exchange rate between dissolved and adsorbed NEA seen in our data is expected to be slow, even if it is still operative. In spite of the presumed hydrogen bonding that may occur between amine groups within the adsorbed NEA, the individual molecules can be replaced by new adsorbates, and the overall enantiocomposition of the NEA adsorbed layer can be reversibly switched between enantiopure (that is, composed of one single enantiomer) and racemic.

4. PO adsorption on Pt(111) under UHV

The second system studied here in connection with the role of enantiocomposition on the properties of adsorbed layers was that of the uptake of propylene oxide (PO) on Pt(111) single-crystal surfaces under ultrahigh vacuum (UHV) conditions. PO is one of the smallest

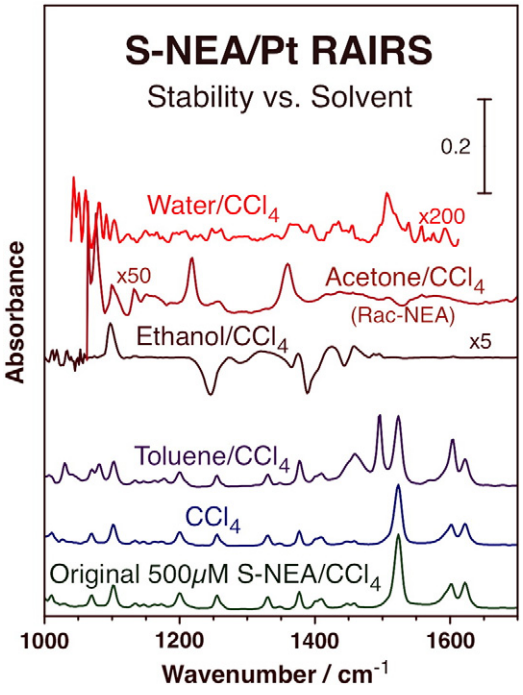

Fig. 4. RAIRS data for S-NEA, right after adsorption from a 500 μM CCl_4 solution on the Pt surface (bottom, green trace) and after flushing with different fresh liquid solvents, namely, from bottom to top: CCl_4, toluene, ethanol, acetone (where Rac-NEA was used instead of S-NEA), and water. In all cases, the surface was also flushed with fresh pure CCl_4 before taking the RAIRS data in order to remove most of the solvent and minimize its interference in the IR spectra. The data indicate that adsorption is less reversible with non-polar solvents (CCl_4, toluene), but that the adsorbate can be easily removed from the surface with polar solvents (ethanol, acetone, water).

molecules that can exist in two enantiomeric forms, and has received some attention recently by the surface-science community because of its value as a probe for chiral sites on surface templated with other chiral agents. The idea was introduced first by Tysoe and coworkers, who showed that, for the case of Pd(111) surfaces pre-dosed with 2-butanol (2-ButOH), the total uptake of PO, that is, the extent of the availability of empty sites, varies significantly depending on the combinations of enantiomers used, with homochiral pairs (R-PO on R-2-ButOH/Pd(111) layers or S-PO on S-2-ButOH/Pd(111) layers) showing PO monolayer saturation coverages up to twice as large as those obtained with heterochiral pairs (R-PO on S-2-ButOH/Pd(111) layers or S-PO on R-2-ButOH/Pd(111) layers) [20]. This difference is only seen for intermediate coverages of 2-ButOH, and reaches its maximum on Pd(111) at 2-ButOH coverages of approximately half a monolayer. That observation strongly suggests a concerted supramolecular effect where the initial chiral molecules (2-ButOH) form templates with a limited number of enantioselective sites. Similar studies have since been carried out with other templating molecules [46] and on other metal surfaces [19,21–23,44,47–49]. However, to the best of our knowledge, there have been no studies on the enantiodependence of the uptake of PO alone on metal surfaces. We have only recently started to investigate this issue [26]; below we report on new data relevant to that discussion.

It was found that the total monolayer coverage of PO that can be reached at low temperatures on Pt(111) surfaces varies significantly, by as much as 20%, depending on the ratio of S-PO to R-PO in that layer. This can be clearly seen in temperature-programmed desorption (TPD) data by the variations in the total area of the peak associated with molecular desorption from that monolayer, which is centered around 195 K (additional desorption from condensed multilayers is seen at ~150 K) [21]. Fig. 5 displays typical TPD traces to illustrate this point. Three sets of experiments are reported, for surfaces dosed sequentially with x L of S-PO plus (2 − x) L of R-PO (left panel), with the reverse x L of R-PO plus (2 − x) L of S-PO combination (center), and with x L of S-PO plus (2 − x) L of Rac-PO (right). In all three cases, changes in signal intensities are evident as the exposure of the first adsorbate (the x in the description of the experiments above) is varied, with minima in TPD peak areas obtained at intermediate values of x, approximately 0.5 L, in the first two cases (and with x = 0 after Rac-PO predosing). It is also apparent that the shape of the TPD peaks changes with PO monolayer enantiocomposition, with the layers made with racemic mixtures displaying narrow peaks and those with high fractions of one of the enantiomers showing an additional high-temperature tail. The differences in peak shape are subtle but consistent, outside our experimental error, and are an indication of slight changes in adsorption energies with coverages. However, that information is difficult to extract from these data, and is better evaluated by using the molecular beam experiments reported below.

Quantitation of the chiral behavior reported above was done by estimating the total PO surface coverages from the areas of the TPD peaks and plotting those versus the coverage of one of the two PO enantiomers, S-PO in the figures provided in this report. Some of the key results from such analysis are summarized in Fig. 6. The data can in fact be displayed in several ways depending on the emphasis desired. Specifically, the total PO monolayer coverages can be analyzed as a function of the initial coverage of the enantiomer dosed first, which can be calibrated independently with simple TPD experiments versus exposure using one single version of the PO (enantiopure S- or R-PO, or Rac-PO); the solid green circles in Fig. 6 show the result from this type of analysis for the case of the x L of S-PO plus (2 − x) L of R-PO dosing sequence. Looked at it this way, the minimum in PO monolayer saturation coverage is seen for an initial S-PO coverage of ~60% of a monolayer. At first sight, such result may suggest a slight asymmetry in the way the S-PO + R-PO layers develop during the sequential dosing experiments. However, this effect is not real, because some molecular displacement of adsorbed PO molecules takes place during dosing of the second PO. The extent of that displacement was estimated by us before by using PO-d_0 + PO-d_6 dosing combinations (since those can be distinguished in the TPD thanks to their different molecular mass) [26], and used here to estimate the final coverages of the first PO enantiomer after dosing of the second. The new set of data, for the PO saturation coverage versus the final coverage of S-PO, is reported in Fig. 6 as open blue circles for the same x L of S-PO plus (2 − x) L of R-PO case as before. Under this new analysis, the minimum PO monolayer saturation coverage is obtained for a final 50:50 S-PO:R-PO mixture. Analogous data obtained using either Rac-PO-d_0 (solid red squares, from the data in the right panel of Fig. 5) or Rac-PO-d_6 (open purple squares) show similar trends.

It should be pointed out that although most of the PO adsorbed on the Pt(111) surface desorbs molecularly and is detected in the 195 K molecular TPD peak shown in Fig. 5, a small fraction decomposes on the surface and is not reflected in the area of that TPD feature [21].

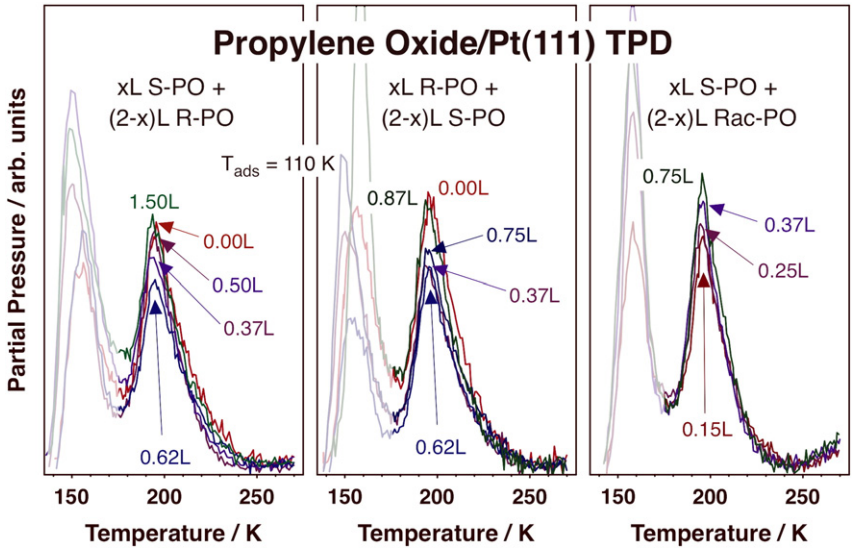

Fig. 5. Representative temperature-programmed desorption (TPD) data for the molecular desorption (58 amu) of propylene oxide (PO) from Pt(111) single-crystal surfaces after 2.0 L total doses at 110 K. The traces correspond to different combinations of sequential dosings with enantiopure and racemic mixtures of PO: x L S-PO + (2.0 − x) L R-PO (left frame), x L R-PO + (2.0 − x) L S-PO (center), and x L S-PO + (2.0 − x) L Rac-PO (right). The areas of the molecular desorption TPD peak from the monolayer, the feature at ~195 K, were used to determine the corresponding saturation coverages; they were seen to vary significantly depending on the final enantiocomposition of the PO monolayer.

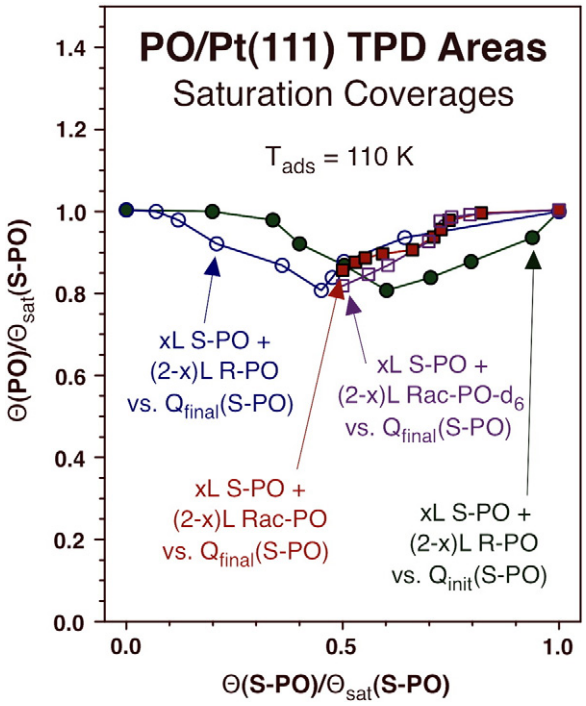

Fig. 6. Summary of TPD area data from experiments such as those reported in Fig. 5 for surfaces first dosed with varying amounts of S-PO and then with R-PO (open blue circles and green solid circles), Rac-PO-d_0 (solid red squares), or Rac-PO-d_6 (open purple squares). The data are shown as a function of the surface coverage of S-PO, estimated by an independent calibration of coverage versus exposure. The final S-PO coverages, estimated from additional experiments with isotope-labeled PO [26], were used to plot the data in all three cases, but an additional trace is shown as a function of the initial S-PO coverage for the S-PO + R-PO case (green solid circles) to highlight the fact that some S-PO is displaced by new PO molecules during the second half of the experiments. After correcting for that effect, it is seen that the PO saturation coverage reaches a minimum value for monolayers with approximately 50:50 S-PO:R-PO composition regardless of how they are produced. That coverage is about 20% lower than that of the saturation layers reached with enantiopure PO.

However, this decomposition amounts to only approximately 10% of a monolayer, and can be quantified by using the TPD traces obtained for the molecular hydrogen that results from the eventual total dehydrogenation of the surface species. Such analysis indicated that the coverages of the PO that decomposes on the surface follow the same trends as a function of the enantiocomposition of the PO monolayer as those seen in the molecular TPD data (data not shown). The addition of both molecular and H_2 TPD areas, to estimate the true initial coverage of PO, leads to plots with the same trends as those reported in Fig. 6.

Several features make this PO/Pt(111) system quite unique, and differentiate it from past studies with other chiral adsorbates [26]. First, PO is not a molecule prone to form hydrogen bonds, and no evidence of such intermolecular interactions was seen in STM images of PO monolayers on Pt(111) [26]. A second observation from the STM studies is that the PO layers do not display any long-range order, as is the case with many of the other reported cases with chiral adsorbates. Third, the facts that the total PO saturation coverage variations evidenced in Fig. 6 occur progressively as a function of the variations in S-PO:R-PO monolayer composition and that the same results are obtained regardless of the way the different enantiomers are added to the surface, either sequentially or by using a racemic mixture, suggest that the final PO monolayers are surface solutions of the S-PO and R-PO components, not racemates or conglomerates of separate homochiral domains. Fourth, it is curious that it is the mixed S-PO + R-PO monolayers the one that display lower monolayer densities; the majority of examples of chiral mixtures in two- and three-dimensions show the opposite trend (with the lowest density obtained with the enantiopure samples) [50]. Fifth, the changes in PO monolayer density with enantiocomposition do not translate in appreciable changes in desorption energy, given that the TPD peaks are all centered around the same temperature (although the high-temperature tails may indicate changes in desorption kinetics at lower coverages, as mentioned before); typically, higher (or lower) densities in chiral solids, are accompanied by higher (or lower) melting points [51]. Finally, the chiral effects reported here are seen at all adsorption temperatures up to the point where the monolayers desorb, close to 200 K, but becomes less pronounced at the high-temperature end of that range.

All these observations indicate that the behavior we report for the PO monolayers on Pt(111) is most likely the result of kinetic, not thermodynamic, effects. This idea has been corroborated by the isothermal sticking coefficient (S) results obtained from so-called King and Wells experiments with a molecular beam setup [29,52]. Fig. 7 shows the sticking coefficients measured at 160 K for S- (left panel), Rac- (center), and R- (right) PO as a function of total PO surface coverage on Pt(111) surfaces predosed with different amounts of S-PO. Several clear trends can be extracted from these data. First, for the same combination of exposures in the two dosing steps of these experiments, lower sticking coefficients are seen with the heterochiral combination (S-PO followed by R-PO) than with the homochiral counterpart (S-PO on S-PO/Pt(111)); the experiment where Rac-PO is added typically falls in between the other two (the differences are small and close to the experimental errors, but the trends are systematic). This goes together with the corresponding reductions in total PO coverages reached, in which these molecular-beam results corroborate the trends identified by TPD. In addition, all the sticking coefficient traces, for all initial S-PO doses, track each other (within experimental error) in the high-coverage end of the uptake with the S-PO + S-PO experiment, as expected, but they deviate in the mixed-enantiomer cases, shifting to lower S values with increasing initial S-PO dose. Again, this correlates with the fact that in those cases the system reaches lower total PO saturation coverages.

One additional observation from the molecular beam data, also reported in our initial report [26], is that, in all cases, the sticking coefficient increases with coverage in the initial stages of the uptake. This is unusual, but has been observed in a few selected systems in the past, and explained by adsorption dynamics assisted by adsorbates already present on the surface [53,54]. The validity of that hypothesis in our case was tested in Monte Carlo simulations, which were set to use two different adsorption probabilities on empty versus PO-nearest-neighbor sites on the surface (the latter being much higher), and also to require different adsorption geometries for adjacent PO adsorbates depending on their relative chirality [26]. Data from those simulations, designed to match the experimental conditions reported in Fig. 7, are provided in Fig. 8. They qualitatively reproduce the main observations cited above, namely, the lower values of the sticking coefficients and final saturation coverages obtained with heterochiral S-PO + R-PO mixtures (compared to the homochiral S-PO + S-PO case), the deviations in the high-coverage side of the curves from the original behavior seen on clean Pt(111) when different chiral compositions are used for the first and second dosings within a single experiment, and the increases in sticking coefficient with increasing surface PO coverages in the initial stages of the uptake. It would appear that our kinetic model explains the behavior seen in the experiments reported here.

5. Conclusions

In this report, we have provided data for two different adsorption systems of chiral molecules on platinum surfaces where the uptake and nature of the resulting monolayers vary in detectable ways depending on their enantiomeric composition. Other than sharing the same metal as the substrate, the two systems are quite different: they involved very different molecules, namely a simple structure (PO) versus a more complex organic compound capable of bestowing enantioselectivity to

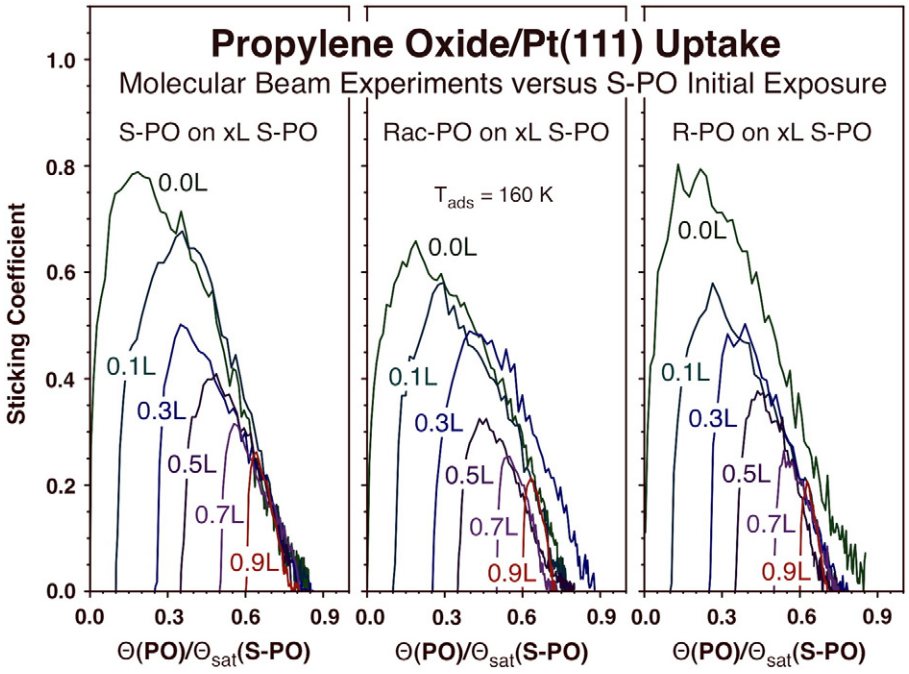

Fig. 7. Isothermal uptake curves, in the form of sticking coefficient versus total PO surface coverage, for S-PO on Pt(111) surfaces predosed with varying amounts of S- (left panel), Rac- (center), or R- (right) PO. The data were all acquired at a surface temperature of 160 K by using an effusive molecular beam setup [29]. Two important observations derive from these data: (1) the sticking coefficient increases with coverage in the early stages of the uptake, suggesting an adsorbate-assisted adsorption process; and (2) under equivalent conditions, the sticking coefficients are lower for hetero- (versus homo-) enantiomer combinations, indicating a different interaction between the incoming and adsorbed PO molecules depending on their relative handedness (S/S or R/R versus S/R or R/S).

hydrogenation catalysts (NEA), and were exposed to very different environments, ultrahigh vacuum (UHV) in the case of PO and a liquid solution with NEA. As a consequence, they also show a somewhat different behavior, although that may be explained, at least in part, by the different nature of the two experiments. Nevertheless, the common feature in both cases is the changes that are seen on the adsorbed monolayers as a function of their enantiomeric composition.

In the case of the NEA adsorption on Pt surfaces from CCl_4 solutions, in situ infrared absorption spectra indicated a different adsorption mode for enantiopure versus racemic monolayers. Previous work in our laboratory suggested that bonding in this case most likely involves the amine group of the NEA, and the data reported here added information on the possible hydrogen bonding between adjacent molecules, with a different character with homochiral (S-NEA/S-NEA or

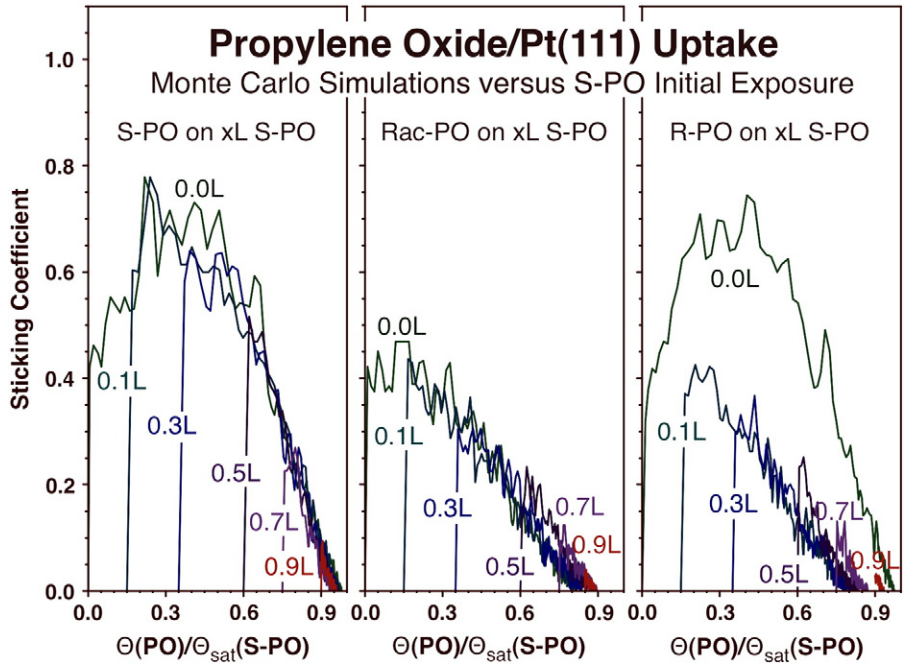

Fig. 8. Results from Monte Carlo simulations of the experiments described in Fig. 7. The main qualitative trends seen in the experimental data could be reproduced by incorporating two assumptions in the simulations: (1) a higher sticking probability on occupied sites, S_o (occupied) = 0.99, than on empty sites, S_o (empty) = 0.01; and (2) an enantiospecific geometry for the PO molecules that adsorb next to other PO adsorbates, different for cases involving the same versus the opposite chirality [26].

R-NEA/R-NEA) versus with heterochiral (S-NEA/R-NEA or R-NEA/S-NEA) pairs of adsorbates. The proposal is that the racemic layer may consist of S–R racemates bonded together via hydrogen bonding. It was also determined that NEA adsorption under these conditions is reversible, and that NEA molecules from solution are capable of displacing other NEA molecules bonded to the surface. The exchange is slow in non-polar solvents such as the CCl_4 used here (or toluene), but straight NEA desorption was shown to occur readily with polar solvents such as ethanol, acetone, or water, in which case total removal of the NEA monolayer with fresh solvent is quite facile. When using molecules of different chirality, the average enantiomeric composition of the saturated NEA monolayers can be transitioned from 100% of one enantiomer to a racemic mixture and back. However, the lack of evidence for additional intermolecular interactions suggests the existence of enantiopure and racemic conglomerates on the surface preferentially exchanging NEA molecules with those in solution at the domain boundaries.

The study on the uptake of PO on Pt(111) surfaces was carried out under vacuum and by using TPD and molecular beam experiments, but also provided evidence for differences due to the enantiocomposition of the PO monolayers. In this case, less dense saturation monolayers were detected with mixed-chirality layers, with the values for PO racemic mixtures being about 20% lower than those obtained with enantiopure S-PO or R-PO. In spite of having performed the experiments under UHV conditions, significant displacement of the adsorbates by PO molecules coming from the gas phase was seen in this system as well. The observed behavior with PO is explained by kinetic, not thermodynamic, effects. It was found that the adsorption is assisted by other surface adsorbates, and that such behavior leads to initial increases in sticking probabilities at the early stages of the dosing. Moreover, lower sticking coefficients are always seen with heterochiral combinations of incoming molecules and adsorbates, a trend that could be reproduced in Monte Carlo simulations by proposing different relative geometrical configurations for homochiral (S-PO/S-PO or R-PO/R-PO) versus heterochiral (S-PO/R-PO or R-PO/S-PO) pairs.

To reiterate, two very different chiral molecules were shown to display changing behavior on solid surfaces depending on their enantiomeric composition. It is quite possible that such differences are common; the lack of additional examples in the literature to date may most likely be due to a lack of studies on such chirality-dependent monolayers. This type of behavior is expected to have important consequences in both two- and three-dimensional systems, in fields such as preferential crystallization and enantioselective catalysis, but the details are missing at present because of our limited knowledge in this area. It is hoped that an increased enthusiasm for the characterization of chiral adsorbates by the surface-science community may correct his deficiency in the near future.

Acknowledgments

Financial support for this project was provided by the U.S. Department of Energy, Office of Basic Energy Sciences, Grant DE-FG02-12ER16330.

References

[1] R. Raval, Chem. Soc. Rev. 38 (2009) 707.
[2] Z. Ma, F. Zaera, in: U.S. Ozkan (Ed.), Design of Heterogeneous Catalysis: New Approaches Based on Synthesis, Characterization, and Modelling, Wiley-VCH, Weinheim, 2009, p. 113.
[3] K.H. Ernst, Phys. Status Solidi B 249 (2012) 2057.
[4] M. Parschau, S. Romer, K.H. Ernst, J. Am. Chem. Soc. 126 (2004) 15398.
[5] C. Roth, D. Passerone, K.H. Ernst, Chem. Commun. 46 (2010) 8645.
[6] K.H. Ernst, Orig. Life Evol. Biosph. 40 (2010) 41.
[7] M. Parschau, R. Fasel, Ernst K. H., Cryst. Growth Des. 8 (2008) 1890.
[8] S. Haq, N. Liu, V. Humblot, A.P.J. Jansen, R. Raval, Nat. Chem. 1 (2009) 409.
[9] A.G. Mark, M. Forster, R. Raval, Tetrahedron Asymmetry 21 (2010) 1125.
[10] G. Coquerel, Top. Curr. Chem. 269 (2007) 1.
[11] G. Webb, P.B. Wells, Catal. Today 12 (1992) 319.
[12] M. Studer, H.U. Blaser, C. Exner, Adv. Synth. Catal. 345 (2003) 45.
[13] T. Mallat, E. Orglmeister, A. Baiker, Chem. Rev. 107 (2007) 4863.
[14] T. Osawa, T. Harada, O. Takayasu, Curr. Org. Chem. 10 (2006) 1513.
[15] P.B. Wells, A.G. Wilkinson, Top. Catal. 5 (1998) 39.
[16] E. Schmidt, C. Bucher, G. Santarossa, T. Mallat, R. Gilmour, A. Baiker, J. Catal. 289 (2012) 238.
[17] S. Lavoie, M.A. Laliberte, I. Temprano, P.H. McBreen, J. Am. Chem. Soc. 128 (2006) 7588.
[18] A. Baiker, J. Mol. Catal. A Chem. 115 (1997) 473.
[19] F. Zaera, J. Phys. Chem. C 112 (2008) 16196.
[20] D. Stacchiola, L. Burkholder, W.T. Tysoe, J. Am. Chem. Soc. 124 (2002) 8984.
[21] I. Lee, F. Zaera, J. Phys. Chem. B 109 (2005) 12920.
[22] I. Lee, F. Zaera, J. Am. Chem. Soc. 128 (2006) 8890.
[23] I. Lee, Z. Ma, S. Kaneko, F. Zaera, J. Am. Chem. Soc. 130 (2008) 14597.
[24] L. Burkholder, D. Stacchiola, J.A. Boscoboinik, W.T. Tysoe, J. Phys. Chem. C 113 (2009) 13877.
[25] F. Gao, Y. Wang, L. Burkholder, W.T. Tysoe, J. Am. Chem. Soc. 129 (2007) 15240.
[26] S. Karakalos, T.J. Lawton, F.R. Lucci, E.C.H. Sykes, F. Zaera, J. Phys. Chem. C 117 (2013) 18588.
[27] J. Kubota, Z. Ma, F. Zaera, Langmuir 19 (2003) 3371.
[28] J. Liu, M. Xu, T. Nordmeyer, F. Zaera, J. Phys. Chem. 99 (1995) 6167.
[29] F. Zaera, Int. Rev. Phys. Chem. 21 (2002) 433.
[30] M.J. Frisch, G.W. Trucks, H.B. Schlegel, G.E. Scuseria, M.A. Robb, J.R. Cheeseman, G. Scalmani, V. Barone, B. Mennucci, G.A. Petersson, H. Nakatsuji, M. Caricato, X. Li, H.P. Hratchian, A.F. Izmaylov, J. Bloino, G. Zheng, J.L. Sonnenberg, M. Hada, M. Ehara, K. Toyota, R. Fukuda, J. Hasegawa, M. Ishida, T. Nakajima, Y. Honda, O. Kitao, H. Nakai, T. Vreven, J.J.A. Montgomery, J.E. Peralta, F. Ogliaro, M. Bearpark, J.J. Heyd, E. Brothers, K.N. Kudin, V.N. Staroverov, T. Keith, R. Kobayashi, J. Normand, K. Raghavachari, A. Rendell, J.C. Burant, S.S. Iyengar, J. Tomasi, M. Cossi, N. Rega, J.M. Millam, M. Klene, J.E. Knox, J.B. Cross, V. Bakken, C. Adamo, J. Jaramillo, R. Gomperts, R.E. Stratmann, O. Yazyev, A.J. Austin, R. Cammi, C. Pomelli, J.W. Ochterski, R.L. Martin, K. Morokuma, V.G. Zakrzewski, G.A. Voth, P. Salvador, J.J. Dannenberg, S. Dapprich, A.D. Daniels, O. Farkas, J.B. Foresman, J.V. Ortiz, J. Cioslowski, D.J. Fox, Gaussian 09, Revision B.01, Gaussian, Inc., Wallingford CT, 2010.
[31] S. Diezi, M. Hess, E. Orglmeister, T. Mallat, A. Baiker, J. Mol. Catal. A Chem. 239 (2005) 49.
[32] V. Demers-Carpentier, G. Goubert, F. Masini, R. Lafleur-Lambert, Y. Dong, S. Lavoie, G. Mahieu, J. Boukouvalas, H. Gao, A.M.H. Rasmussen, L. Ferrighi, Y. Pan, B. Hammer, P.H. McBreen, Science 334 (2011) 776.
[33] L. Burkholder, M. Garvey, M. Weinert, W.T. Tysoe, J. Phys. Chem. C 115 (2011) 8790.
[34] T. Heinz, G. Wang, A. Pfaltz, B. Minder, M. Schuerch, T. Mallat, A. Baiker, J. Chem. Soc. Chem. Commun. (1995) 1421.
[35] E. Orglmeister, T. Mallat, A. Baiker, Adv. Synth. Catal. 347 (2005) 78.
[36] E. Tálas, J.L. Margitfalvi, Chirality 22 (2010) 3.
[37] J.M. Bonello, F.J. Williams, R.M. Lambert, J. Am. Chem. Soc. 125 (2003) 2723.
[38] S. Lavoie, M.-A. Laliberté, P.H. McBreen, J. Am. Chem. Soc. 125 (2003) 15756.
[39] J.A. Boscoboinik, Y. Bai, L. Burkholder, W.T. Tysoe, J. Phys. Chem. C 115 (2011) 16488.
[40] A.D. Gordon, F. Zaera, Angew. Chem. Int. Ed. 52 (2013) 3453.
[41] Z. Ma, F. Zaera, J. Am. Chem. Soc. 128 (2006) 16414.
[42] Z. Ma, I. Lee, F. Zaera, J. Am. Chem. Soc. 129 (2007) 16083.
[43] Z. Ma, F. Zaera, J. Phys. Chem. B 109 (2005) 406.
[44] F. Zaera, Acc. Chem. Res. 42 (2009) 1152.
[45] L. Mink, Z. Ma, R.A. Olsen, J.N. James, D.S. Sholl, L.J. Mueller, F. Zaera, Top. Catal. 48 (2008) 120.
[46] D. Stacchiola, L. Burkholder, T. Zheng, M. Weinert, W.T. Tysoe, J. Phys. Chem. B 109 (2005) 851.
[47] F. Gao, Y. Wang, Z. Li, O. Furlong, W.T. Tysoe, J. Phys. Chem. C 112 (2008) 3362.
[48] W.Y. Cheong, Y. Huang, N. Dangaria, A.J. Gellman, Langmuir 26 (2010) 16412.
[49] J.L. Sales, V. Gargiulo, I. Lee, F. Zaera, G. Zgrablich, Catal. Today 158 (2010) 186.
[50] C.P. Brock, W.B. Schweizer, J.D. Dunitz, J. Am. Chem. Soc. 113 (1991) 9811.
[51] H.O. Sørensen, S. Larsen, Acta Crystallogr. B 59 (2003) 132.
[52] D.A. King, M.G. Wells, Surf. Sci. 29 (1972) 454.
[53] M. Bowker, D.A. King, J. Chem. Soc. Faraday Trans. 1 (75) (1979) 2100.
[54] C.R. Arumainayagam, M.C. McMaster, R.J. Madix, J. Phys. Chem. 95 (1991) 2461.